

Proteome selectivity profiling of photoaffinity probes derived from imidazopyrazine-kinase inhibitors

Dimitris Korovesis,¹ Christel Mérellat,¹ Rita Derua^{2,3} and Steven H. L. Verhelst^{1,*}

¹ KU Leuven – University of Leuven, Laboratory of Chemical Biology, Department of Cellular and Molecular Medicine, Herestraat 49 box 901b, 3000 Leuven, Belgium

² KU Leuven – University of Leuven, Laboratory of Protein Phosphorylation and Proteomics, Department of Cellular and Molecular Medicine, Herestraat 49 box 901, 3000 Leuven, Belgium

³ KU Leuven, SyBioMa, Herestraat 49, 3000 Leuven, Belgium

Abstract

Kinases are attractive drug targets, but the design of highly selective kinase inhibitors remains challenging. Selectivity may be evaluated against a panel of kinases, or – preferred – in a complex proteome. Probes that allow photoaffinity-labeling of their targets can facilitate this process. Here, we report photoaffinity probes based on the imidazopyrazine scaffold, which is found in several kinase inhibitors and drugs or drug candidates. By chemical proteomics experiments, we find a range of off-targets, which vary between the different probes. *In silico* analysis suggests that differences between probes may be related to the size, spatial arrangement and rigidity of the imidazopyrazine and its substituent at the 1-position.

Introduction

Protein phosphorylation, catalyzed by protein kinases, represents one of the most common post-translational modifications (PTMs) and regulates a wide variety of signaling networks in the cell.¹ Changes in protein phosphorylation mediate processes such as transcription, apoptosis, metabolism, cell proliferation and cell differentiation.^{1,2} Unsurprisingly, dysregulation of kinase activity contributes to various human pathologies, including inflammatory diseases,³ neurodegenerative diseases⁴ and cancer.⁵

The human genome codes for more than 500 kinases,² which are subdivided into 7 subgroups (Figure 1A). The kinase domains consist of 2 lobes; the N- and the C-terminal lobe, connected by a hinge region (Figure 1B). The ATP-binding pocket is located between the two lobes, and the substrate binding site locates to the C-terminal lobe. Interactions at this site determine – in part – the selectivity of kinases towards certain substrates.⁶ Because of their role in various human diseases, kinase inhibitors have received a lot of attention from drug discovery programs. This has been quite successful: approximately 80 kinase inhibitors have been approved by the Food and Drug Administration (FDA), predominantly for treatment of cancer.⁷ Nevertheless, the development of selective kinase inhibitors remains highly challenging. One of the main reasons is that most kinase inhibitors mimic the ATP structure and bind into the conserved ATP binding site. Many medicinal chemistry efforts have focused on small differences in the ATP binding site in order to develop kinase inhibitors that are selective for a kinase target of interest.⁸ Oppositely, there is also evidence that a certain degree of promiscuity – i.e. targeting multiple kinase targets – may be beneficial for treatment of disease because of redundancies of kinases involved in signaling pathways.⁹

Various mass spectrometry (MS) techniques exist to identify the target(s) of a kinase inhibitor from whole proteomes. The benefit is that some of these techniques also identify non-kinase targets. They include thermal proteome profiling,¹⁰ kinobeads,^{11,12} and photoaffinity labeling (PAL).¹³ Through a PAL approach, we have recently shown that the imidazo[1,5-a]pyrazine-based kinase inhibitor KIRA6 (Figure 1C), which is a reported inhibitor of IRE1 α ,¹⁴ has a wide range of other non-kinase targets,¹⁵ including the ATP-binding HSP60.¹⁶ Interestingly, the imidazopyrazine core structure occurs in the FDA-approved drug acalabrutinib, which inhibits Bruton's tyrosine kinase (BTK), drug candidate linsitinib, which targets insulin-like growth factor 1 receptor (IGF-1R) (Figure 1D), and several other reported kinase inhibitors, for example for activated Cdc42-associated kinase (ACK1),¹⁷ and *plasmodium falciparum* calcium-dependent protein kinase 1.¹⁸ To provide more insight into the selectivity of this scaffold and how it is influenced by the different substituents, we designed, synthesized and evaluated several imidazopyrazine photoaffinity probes. In line with our previous study,¹⁵ we found that imidazopyrazine-based small molecules target proteins outside

the kinome. *In silico* analysis further suggests that their proteome selectivity (i.e. the number of off-targets) is likely influenced by the size and rigidity of the substituents interacting with the binding pocket (C1 substituent), as well as the overall three-dimensional conformation in solution. Overall, the presented data may offer insight on how to tune the proteome selectivity of imidazopyrazine-based inhibitors.

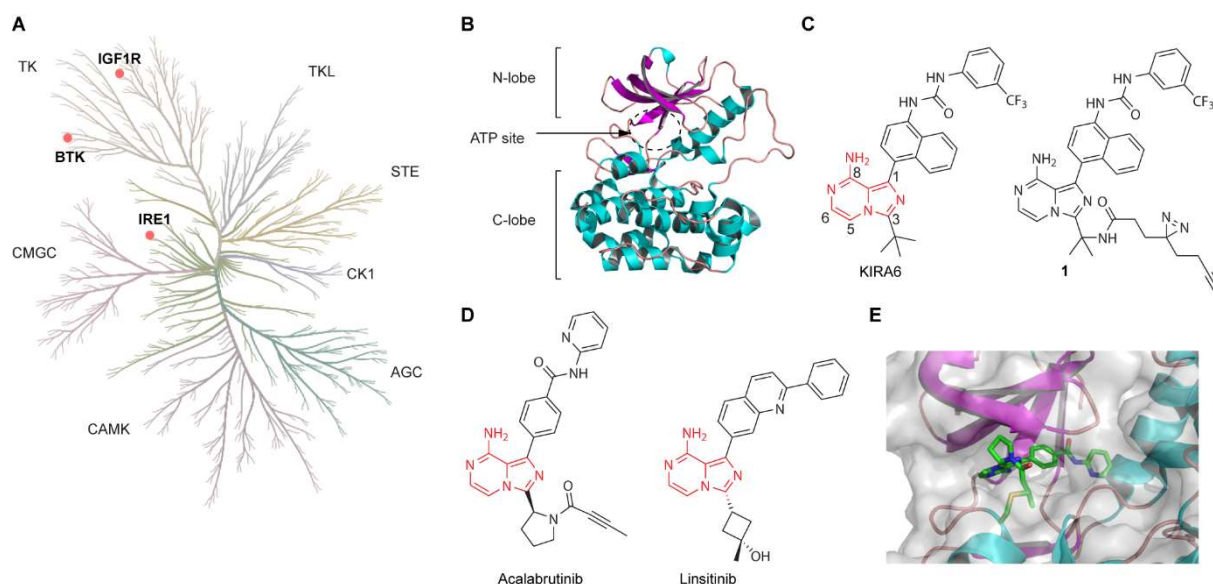


Figure 1. Kinases and imidazopyrazine inhibitors. (A) Kinome tree with indication of BTK, IRE1 and IGF1R, and the 7 kinase subgroups (TK = tyrosine kinases; TKL = TK-like kinases; STE = STE kinases; homologous to yeast STE20, -11, and -7 kinases; CK1 = casein kinase 1 homologues; AGC = protein kinase A, G & C families; CAMK = Ca²⁺/calmodulin-dependent protein kinases, CMGC = diverse group containing cyclin-dependent kinases, mitogen-activated protein kinases, glycogen synthase kinases, and Cdk-like kinases). (B) Structure of a kinase domain (here exemplified by IGF-1R; PDB code: 3D94), with indication of the N- and C-lobes and the ATP-binding pocket. Protein in cartoon mode with helices in cyan, β -sheets in magenta and random coils in pink. Picture rendered with PyMol.¹⁹ (C) Structure of KIRA6 with indicated numbering of the imidazopyrazine scaffold, and the KIRA6-derived photoaffinity probe **1**. (D) Structures of acalabrutinib and linsitinib. (E) Co-crystal structure of acalabrutinib and murine BTK (PDB: 8FD9) reveals that the *N*-substituent on the 5-membered ring points towards the solvent. Acalabrutinib and the covalently-bound cysteine C481 are depicted in sticks, and the protein in cartoon and semi-transparent surface representation. Picture rendered with PyMol.

Results

Besides our already available KIRA6-based photoaffinity probe **1** (Figure 1C), we set out to develop two additional probes that share the imidazopyrazine core, based on the ATP-

competitive kinase inhibitors acalabrutinib and linsitinib. Acalabrutinib is a second generation, irreversible BTK inhibitor that was approved by FDA in 2017.²⁰ It bears a butynamide moiety that covalently reacts with Cys481 located just outside the ATP pocket of BTK. In contrast, linsitinib is a reversible kinase inhibitor – currently in a phase 2 clinical trial (NCT05276063)²¹ – that targets insulin-like growth factor 1 receptor (IGF-1R) and a homologue kinase, the insulin receptor (IR). Both inhibitors exhibited high selectivity for their respective primary targets, when assessed in traditional biochemical assays (against panels of purified protein kinases).^{22,23}

Although acalabrutinib is covalent inhibitor and a clickable derivative could facilitate chemical proteomics studies as done previously for ibrutinib,²⁴ we opted to develop a PAL probe, because this would enable identification of potential non-covalent targets of acalabrutinib. Additionally, it would allow direct comparison with the other PAL probes in this study. Similar to our previous KIRA6 probe **1**,¹⁵ we decided to introduce the same minimalist diazine building block²⁵ at the C3 position of the imidazopyrazine scaffold, because crystal structures of acalabrutinib bound to murine BTK²⁶ (Figure 1E) and of a near-identical linsitinib derivative to IGFR²⁷ (Figure S1) showed that substituents at this position are solvent-exposed. Therefore, the minimalist photoaffinity handle was designed to replace the butynamide moiety on acalabrutinib and the hydroxyl group on linsitinib. For both molecules, the stereochemistry of the C3-substituent on the PAL probes was maintained as in the parent compounds.

The synthesis of the probes is outlined in Figure 2. In brief, chloropyrazine **2** was coupled to Cbz-protected proline (**10a**; for acalabrutinib) or cyclo-butane derivative **10b** (for linsitinib), followed by Bischler-Napieralski cyclization to obtain the imidazopyrazine cores **4a-b**.²⁸ Next, iodination at the C1 position and nucleophilic aromatic substitution of the chlorine by ammonia yielded compounds **6a-b**. Suzuki coupling was employed to introduce the Cx substituent towards **7a-b**. Finally, temporary protection of the exocyclic amine with Fmoc, followed by Cbz removal, coupling with diazine building block **12** and final Fmoc deprotection furnished the desired acalabrutinib-based (**9a**) and linsitinib-based (**9b**) PAL probes.

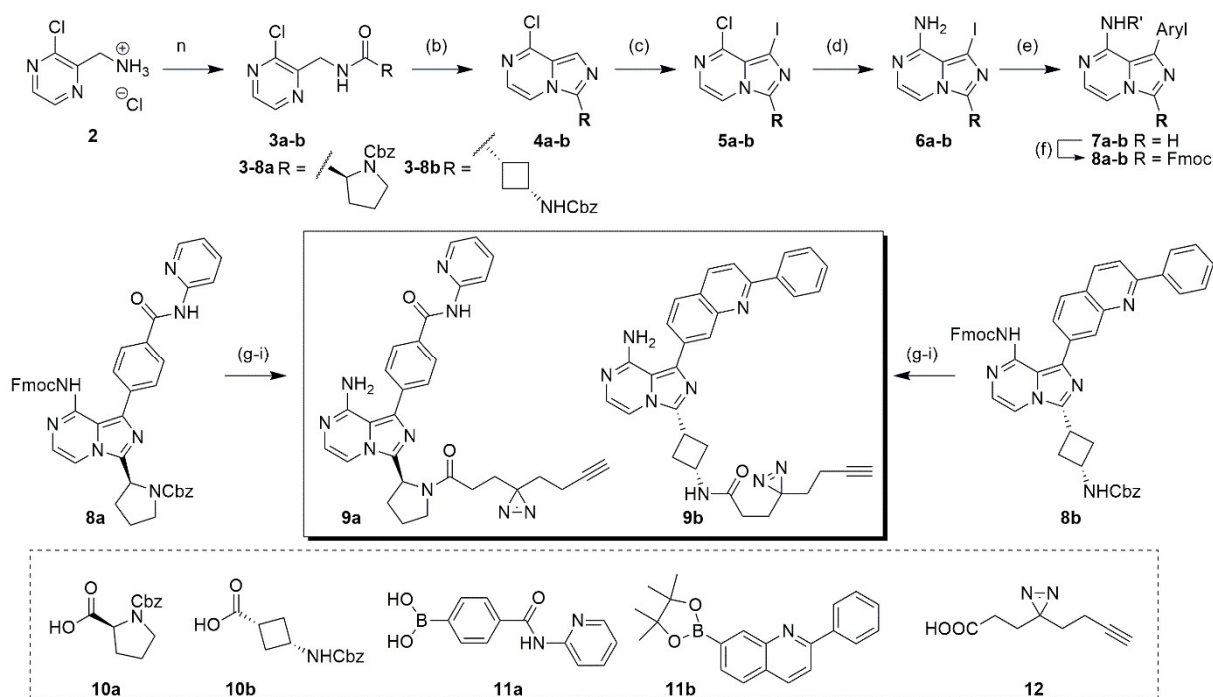


Figure 2. Synthesis of PAL probes **9a** and **9b**. (a) Cmp **10a** or **10b**, EDC.HCl, DCM, rt, o/n.; (b) PCl_5 , MeCN, 0 °C, then 50 °C; (c) *N*-iodo-succinimide, DMF, 60 °C, o/n.; (d) 35% NH_4OH , dioxane, 100 °C. (e) Cmp **11a** or **11b**, K_2CO_3 , $\text{Pd}(\text{PPh}_3)_4$, water/DME, 80 °C, o/n; (f) Fmoc-Cl, pyridine, DCM, rt, o/n. (g) 33% HBr in AcOH, 0 °C, then 1h at rt; (h) Cmp **12**, HATU, DIEA, DMF, rt, o/n; (i) 1% DBU in DMF, 1h, rt.

We next set out to demonstrate the ability of probes **9a-b** to covalently label proteins upon irradiation. To this end, an increasing concentration of probe was incubated in lysates of MCF7 breast cancer cells or Ramos cells, a lymphoma-derived cell line. Irradiation at 365 nm was followed by click chemistry-mediated tagging of the covalently modified proteins with an azido-TAMRA derivative. As expected, an increasing probe concentration led to more intense labeling, which was largely competed out by co-incubation with an excess of the parent kinase inhibitor (Figure 3A). Multiple protein species were labeled by acalabrutinib probe **9a** and linsitinib probe **9b**, which was in line with our previous experiments using KIRA6-based probe **1**.¹⁵ A direct comparison of the three PAL probes in lysates of several different cell lines showed that the overall labeling pattern appeared to be similar, with some minor differences for specific probes and lysates (Figure 3B). For example, in cell lysates of the A375 melanoma cell line, probe **9a** gave labeling of an approximately 30 kDa protein that was not or only weakly labeled by the other probes. This was similar, but less apparent in MCF7 cells. In Ramos cells, probe **1** led to a higher intensity labeling of a protein of approximately 75 kDa. Nevertheless, there appear to be a substantial number of labeled proteins, which represent potential off-targets. Competitive protein profiling experiments using the different probes in competition with

different inhibitors (Figure 3C) showed that not only the parent compound, but also the other imidazopyrazine inhibitors lead to a reduction of labeling intensity, suggesting a (partial) overlap in their targets.

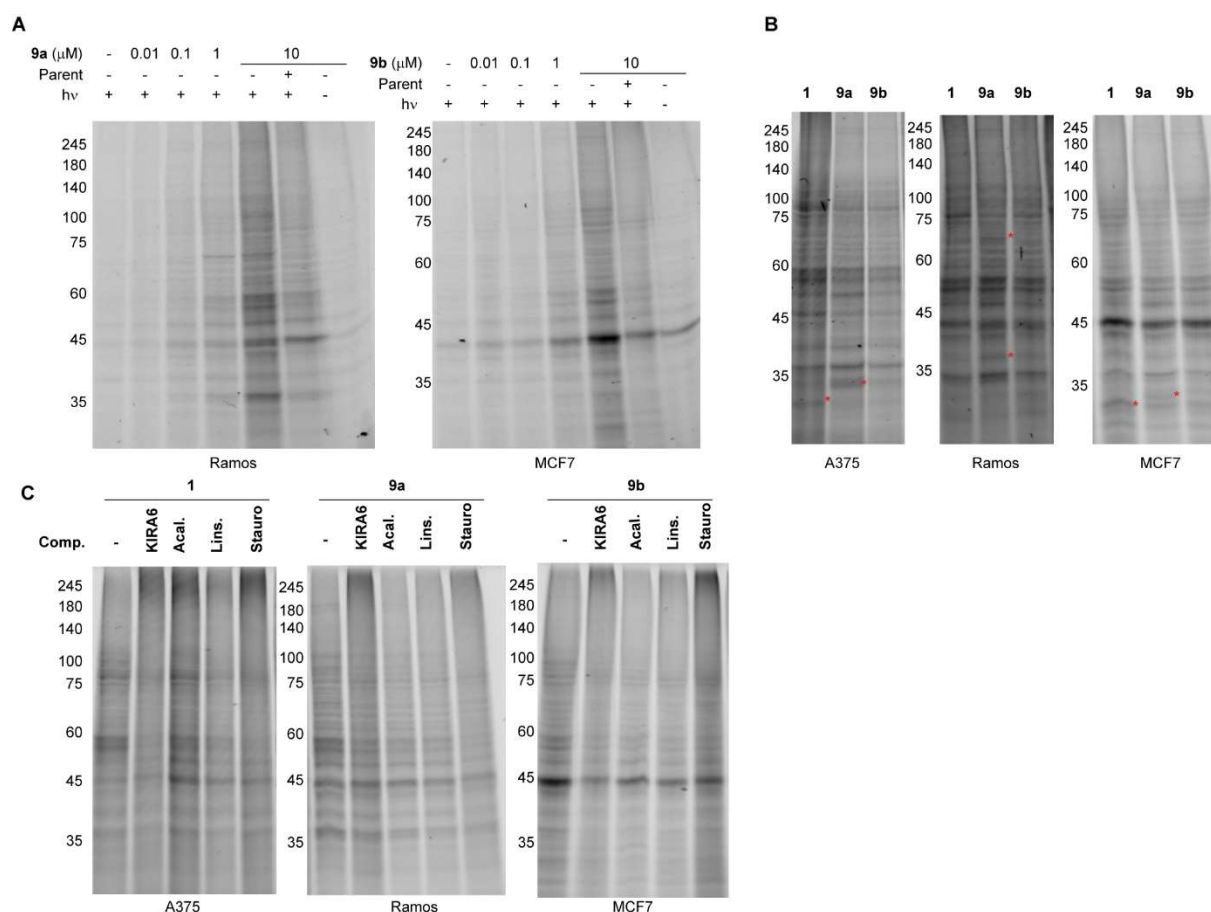


Figure 3. Evaluation of PAL by imidazopyrazine probes **1**, **9a** and **9b**. (A) Increasing labeling intensity by probes **9a** and **9b**, which is largely competed with the parent compound. Click chemistry background (in absence of probe and irradiation) is detected in the most right gel lane. (B) Labeling by the three imidazopyrazine probes in lysates of three different cell lines. Red asterisks indicate some differentially labeled gel bands. (C) Competitive protein profiling in different cell lysates using the parent kinase inhibitors and the pan-kinase inhibitor staurosporin. Coomassie stains of gels in Figures S2-S4.

To identify the imidazopyrazine targets, we followed a chemical proteomics workflow as outlined in Figure 4A. In short, lysates of A431 cells were UV irradiated in the presence of the PAL probe, using DMSO (blank) and PAL probe with excess of parent inhibitor (competition) as controls, and samples were subjected to bioorthogonal click chemistry with a TAMRA-biotin-azide tag (Figure S5 for quality control of replicates). After removal of the excess click reagents, labeled proteins were enriched on immobilized streptavidin. Next, samples were

processed by tryptic digestion before they were analyzed by LC-MS/MS and quantified by label-free quantification (LFQ). Volcano plots of probe versus dms0 (Figure S6) and of probe versus competition (Figure 4B) revealed significant enrichment (2-fold or more) for various proteins (see Table S1 for full lists). We applied stringent selection criteria for hits: proteins were only considered as targets if they were significantly enriched versus both the DMSO and the competition control, and if they were identified with at least two unique peptides. This led to a final target list of 10 proteins for KIRA6 probe **1**, 32 proteins for acalabrutinib probe **9a** and 42 proteins for linsitinib probe **9b** (Table S1), with some overlap in the identified targets (Figure 4C). We classified targets as kinases and nucleotide or nucleoside binding proteins. Since the solvent-exposed diazirine may also react with proteins in very close proximity, we checked for the remaining targets whether they are annotated as kinases interaction partners using the IntAct database (Figure S7).²⁹ Altogether, over half of all targets represent kinases, nucleotide/nucleoside binding or kinase interaction partners (Figure 4D).

KIRA6 probe **1** exhibited the highest selectivity compared with the other imidazopyrazine-based probes. To gain insight in how the molecular structure of the probes may explain their differences we performed MD simulations³⁰ (50 ns in water) of the imidazopyrazine scaffold including the large substituent at the 1-position, which interact with the ATP-binding pocket, but omitting the solvent-exposed 3-substituent (Figure S8). Calculation of the molecular volumes from the MD trajectories (see movies S1-S3) reveals that KIRA6 exhibits the largest three-dimensional size of the three scaffolds and displays a substantial conformational flexibility (Figure 4E, Figure S9). KIRA6 is reported as a type II kinase inhibitor that stabilizes the inactive IRE1 α kinase conformation.¹⁴ Type II inhibitors generally display larger substituents that protrude deep into the ATP binding cleft of the inactive conformation, a feature that was considered to improve selectivity across the kinome.³¹ The larger 1-substituent of KIRA6 may also cause steric conflicts in protein families other than kinases, which could explain the overall lower number of identified targets for the KIRA6 probe **1**.

A principal component analysis of the different conformations of the KIRA6, acalabrutinib and linsitinib scaffolds revealed that linsitinib has a very rigid conformation, in contrast to KIRA6 and acalabrutinib, which occupy a larger conformational space (Figure 4F; see also movies S1-S3). To further explore how the acalabrutinib and linsitinib probes bind to their targets, we decided to perform further *in silico* analysis. To this end, we took all targets identified by proteomics for which crystal structures were available in the Protein Data Bank (2 protein kinases and 8 nucleotide binding proteins) and performed molecular docking using conformations extracted from the MD trajectories as starting points (see methods section in supporting information for details). We consistently found that the linsitinib scaffold displayed higher calculated affinity compared with the acalabrutinib scaffold (Figure S10). These *in silico*

results indicate that the compact structure of linsitinib in solution (Figure 4E), along with the distinct orientation of its substituent (Figure S9), may favor its binding to a higher number of off-targets that bind nucleotides or nucleosides. Additionally, the more rigid linsitinib scaffold with its very defined conformation may undergo a lower entropic penalty when going to the bound state, compared to the highly flexible acalabrutinib (Figure 4F). Collectively, the present study highlights that the proteome selectivity of kinase inhibitors sharing the imidazopyrazine core is likely defined by the size, rigidity and the spatial arrangement of the substituents to be accommodated within a protein pocket.

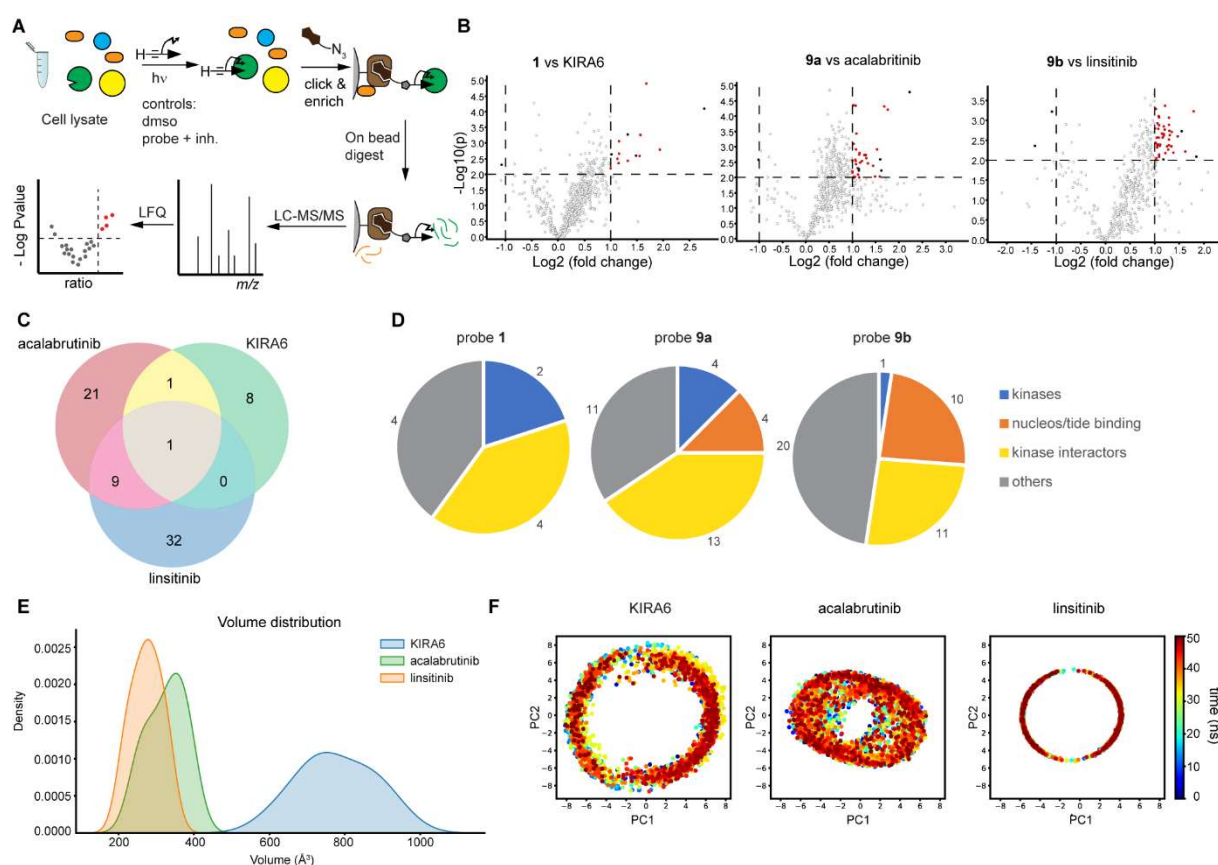


Figure 4. Target identification and analysis. (A) Schematic workflow of the target identification: photoaffinity labeling was followed by click chemistry to introduce a biotin, enrichment on immobilized streptavidin, and on bead digestion. Resulting peptides were analyzed by LC-MS/MS. (B) Volcano plots of significantly enriched proteins in the indicated probe sample versus the competition with the parent inhibitor. 2-fold enrichment and p-value of 0.01 were taken as cut-offs to determine hits in the upper right quadrant. Note that black dots denote proteins that were not significantly enriched in probe versus dms0 (see Figure S6 for volcano plots versus dms0). (C) Venn diagram of the number of targets that were significantly enriched versus dms0 and versus parent inhibitor. (D) Classification of target proteins for each probe – these were classified as kinases, nucleotide or nucleoside binding, kinase interactors or other function. (E) Volume distribution calculated from the MD trajectories. The most frequent

conformation of the KIRA6 scaffold has a bounding box volume of 628 Å³, while the extreme conformations reach up to 998 Å³. In comparison, the other scaffolds show smaller volume ranges, with most frequent conformation volume of 219 Å³ and extreme conformation volumes up to 360 Å³ for the linsitinib scaffold, and a most frequent conformation volume of 351 Å³ and extreme conformation volumes up to 414 Å³ for the acalabrutinib scaffold. (F) principal component analysis of the MD trajectories reveals the largest variation in conformations for acalabrutinib and the smallest variation for linsitinib.

Conclusion

In conclusion, we have synthesized and evaluated novel photoaffinity probes based on imidazopyrazine kinase inhibitors, functionalized with a minimalist diazirine alkyne linker. Using gel-based and chemical proteomics experiments, we showed that these probes display a substantial amount of off-targets. The differences in selectivity may be explained by the size and flexibility of the substituent at the 1-position, and future analysis of a wider set of compounds may provide further evidence for this idea. Moreover, the utilized strategy may be more generally applied for future evaluation of selectivity of other kinase inhibitor scaffolds.

Acknowledgments

We acknowledge funding by the FWO (project grant G0D7118N). We thank L. Baudempez for help with NMR measurements.

Author contributions

D.K. and C.M. synthesized compounds, D.K. and C.M. performed the biochemical experiments, R.D. processed samples for proteomics and performed data analysis, D.K. performed in silico experiments, S.H.L.V. oversaw the project and acquired funding, D.K. and S.H.L.V. wrote the manuscript with input from the other authors.

Competing interests

The authors declare no competing interests.

References

1. Manning, G., Plowman, G. D., Hunter, T. & Sudarsanam, S. Evolution of protein kinase signaling from yeast to man. *Trends in Biochemical Sciences* vol. 27 514–520 (2002).
2. Manning, G., Whyte, D. B., Martinez, R., Hunter, T. & Sudarsanam, S. The protein kinase complement of the human genome. *Science* **298**, 1912–1934 (2002).

3. Cohen, P. Targeting protein kinases for the development of anti-inflammatory drugs. *Current Opinion in Cell Biology* vol. 21 317–324 (2009).
4. Tenreiro, S., Eckermann, K. & Outeiro, T. F. Protein phosphorylation in neurodegeneration: Friend or foe? *Frontiers in Molecular Neuroscience* vol. 7 (2014).
5. Tsai, C. J. & Nussinov, R. The molecular basis of targeting protein kinases in cancer therapeutics. *Seminars in Cancer Biology* vol. 23 235–242 (2013).
6. Ubersax, J. A. & Ferrell Jr, J. E. Mechanisms of specificity in protein phosphorylation. *Nat. Rev. Mol. Cell Biol.* **8**, 530–541 (2007).
7. <http://www.brimr.org/PKI/PKIs.htm>. <http://www.brimr.org/PKI/PKIs.htm>.
8. Attwood, M. M., Fabbro, D., Sokolov, A. V., Knapp, S. & Schiöth, H. B. Trends in kinase drug discovery: targets, indications and inhibitor design. *Nature Reviews Drug Discovery* vol. 20 839–861 (2021).
9. Morphy, R. Selectively nonselective kinase inhibition: striking the right balance. *Journal of Medicinal Chemistry* vol. 53 1413–1437 (2010).
10. Savitski, M. M. *et al.* Tracking cancer drugs in living cells by thermal profiling of the proteome. *Science (80-.)*. **346**, 1255784 (2014).
11. Bantscheff, M. *et al.* Quantitative chemical proteomics reveals mechanisms of action of clinical ABL kinase inhibitors. *Nat. Biotechnol.* **25**, 1035–1044 (2007).
12. Klaeger, S. *et al.* The target landscape of clinical kinase drugs. *Science (80-.)*. **358**, 80–96 (2017).
13. Korovesis, D., Beard, H. A., Mérrillat, C. & Verhelst, S. H. L. Probes for Photoaffinity Labelling of Kinases. *ChemBioChem* vol. 22 2206–2218 (2021).
14. Ghosh, R. *et al.* Allosteric inhibition of the IRE1 α RNase preserves cell viability and function during endoplasmic reticulum stress. *Cell* **158**, 534–548 (2014).
15. Korovesis, D., Rufo, N., Derua, R., Agostinis, P. & Verhelst, S. H. L. Kinase Photoaffinity Labeling Reveals Low Selectivity Profile of the IRE1 Targeting Imidazopyrazine-Based KIRA6 Inhibitor. *ACS Chem. Biol.* **15**, 3106–3111 (2020).
16. Rufo, N. *et al.* Stress-induced inflammation evoked by immunogenic cell death is blunted by the IRE1 α kinase inhibitor KIRA6 through HSP60 targeting. *Cell Death Differ.* **29**, 230–245 (2022).
17. Jin, M. *et al.* Discovery of potent, selective and orally bioavailable imidazo[1,5-a]pyrazine derived ACK1 inhibitors. *Bioorganic Med. Chem. Lett.* **23**, 979–984 (2013).
18. Vidadala, R. S. R. *et al.* Development of potent and selective Plasmodium falciparum calcium-dependent protein kinase 4 (PfCDPK4) inhibitors that block the transmission of malaria to mosquitoes. *Eur. J. Med. Chem.* **74**, 562–573 (2014).
19. Delano, W. L. The Pymol Molecular Graphics Systems (<http://www.pymol.org>). (2002).
20. Byrd, J. C. *et al.* Acalabrutinib (ACP-196) in Relapsed Chronic Lymphocytic Leukemia.

- N. Engl. J. Med.* **374**, 323–332 (2016).
21. No Title. <https://clinicaltrials.gov/study/NCT05276063>.
 22. Barf, T. *et al.* Acalabrutinib (ACP-196): A covalent Bruton tyrosine kinase inhibitor with a differentiated selectivity and in vivo potency profile. *J. Pharmacol. Exp. Ther.* **363**, 240–252 (2017).
 23. Mulvihill, M. J. *et al.* Discovery of OSI-906: A selective and orally efficacious dual inhibitor of the IGF-1 receptor and insulin receptor. *Future Med. Chem.* **1**, 1153–1171 (2009).
 24. Lanning, B. R. *et al.* A road map to evaluate the proteome-wide selectivity of covalent kinase inhibitors. *Nat. Chem. Biol.* **10**, 1–10 (2014).
 25. Li, Z. *et al.* Design and synthesis of minimalist terminal alkyne-containing diazirine photo-crosslinkers and their incorporation into kinase inhibitors for cell- and tissue-based proteome profiling. *Angew. Chemie - Int. Ed.* **52**, 8551–8556 (2013).
 26. Lin, D. Y. & Andreotti, A. H. Structure of BTK kinase domain with the second-generation inhibitors acalabrutinib and tirabrutinib. *PLoS One* **18**, (2023).
 27. Wu, J. *et al.* Small-molecule inhibition and activation-loop trans-phosphorylation of the IGF1 receptor. *EMBO J.* **27**, 1985–1994 (2008).
 28. Bischler, A. & Napieralski, B. Zur Kenntniss einer neuen Isochinolinsynthese. *Berichte der Dtsch. Chem. Gesellschaft* **26**, 1903–1908 (1893).
 29. del Toro, N. *et al.* The IntAct database: efficient access to fine-grained molecular interaction data. *Nucleic Acids Res.* **50**, D648–D653 (2022).
 30. Arantes, P. R., Polêto, M. D., Pedebos, C. & Ligabue-Braun, R. Making it Rain: Cloud-Based Molecular Simulations for Everyone. *J. Chem. Inf. Model.* **61**, 4852–4856 (2021).
 31. Liu, Y. & Gray, N. S. Rational design of inhibitors that bind to inactive kinase conformations. *Nat. Chem. Biol.* **2**, 358–364 (2006).